Magic-Angle Spinning Solid-State NMR Spectroscopy of the β1 Immunoglobulin Binding Domain of Protein G (GB1): 15 N and 13 C Chemical Shift Assignments and Conformational Analysis

ARTICLE *in* JOURNAL OF THE AMERICAN CHEMICAL SOCIETY · OCTOBER 2005

Impact Factor: 12.11 · DOI: 10.1021/ja044497e · Source: PubMed

8 AUTHORS, INCLUDING:

William Trent Franks
The University of Warwick
35 PUBLICATIONS **1,292** CITATIONS
SEE PROFILE

Donghua H Zhou
Oklahoma State University - Stillwater
27 PUBLICATIONS **1,054** CITATIONS
SEE PROFILE

Benjamin J Wylie
Texas Tech University
25 PUBLICATIONS **947** CITATIONS
SEE PROFILE

Chad Michael Rienstra
University of Illinois, Urbana-Champaign
109 PUBLICATIONS **5,600** CITATIONS
SEE PROFILE

J|A|C|S
ARTICLES
Published on Web 08/11/2005

Magic-Angle Spinning Solid-State NMR Spectroscopy of the β1 Immunoglobulin Binding Domain of Protein G (GB1): ^{15}N and ^{13}C Chemical Shift Assignments and Conformational Analysis

W. Trent Franks, Donghua H. Zhou, Benjamin J. Wylie, Brian G. Money, Daniel T. Graesser, Heather L. Frericks, Gurmukh Sahota, and Chad M. Rienstra*

Contribution from the Department of Chemistry, University of Illinois at Urbana-Champaign, 600 South Mathews Avenue, Urbana, Illinois 61801

Received September 10, 2004; E-mail: rienstra@scs.uiuc.edu

Abstract: Magic-angle spinning solid-state NMR (SSNMR) studies of the β1 immunoglobulin binding domain of protein G (GB1) are presented. Chemical shift correlation spectra at 11.7 T (500 MHz ^{1}H frequency) were employed to identify signals specific to each amino acid residue type and to establish backbone connectivities. High sensitivity and resolution facilitated the detection and assignment of every ^{15}N and ^{13}C site, including the N-terminal (M1) $^{15}NH_3$, the C-terminal (E56) $^{13}C'$, and side-chain resonances from residues exhibiting fast-limit conformational exchange near room temperature. The assigned spectra lend novel insight into the structure and dynamics of microcrystalline GB1. Secondary isotropic chemical shifts report on conformation, enabling a detailed comparison of the microcrystalline state with the conformation of single crystals and the protein in solution; the consistency of backbone conformation in these three preparations is the best among proteins studied so far. Signal intensities and line widths vary as a function of amino acid position and temperature. High-resolution spectra are observed near room temperature (280 K) and at $<$180 K, whereas resolution and sensitivity greatly degrade substantially near 210 K; the magnitude of this effect is greatest among the side chains of residues at the intermolecular interface of the microcrystal lattice, which we attribute to intermediate-rate translational diffusion of solvent molecules near the glass transition. These features of GB1 will enable its use as an excellent model protein not only for SSNMR methods development but also for fundamental studies of protein thermodynamics in the solid state.

Introduction

Robust and efficient methods for determining atomic resolution structures of macroscopically disordered proteins are highly sought after, due to the importance of membrane proteins as pharmaceutical targets[1] and the roles that insoluble aggregates of peptides (fibrils) play in neurodegenerative diseases.[2] Beyond the direct implications of atomic resolution data for rational drug design, experimental measurements of structural and dynamic parameters in the solid state enhance the fundamental understanding of protein thermodynamics and provide valuable benchmarks for comparison to theoretical models of protein folding, electrostatics, and dynamics. It is well-known that solid-state NMR (SSNMR) can directly probe anisotropic parameters (such as chemical shift anisotropies and dipolar couplings) of interest to these problems.[3,4] However, the rate at which such data have been extracted from SSNMR spectra has historically been inadequate for site-specific measurements to be made throughout entire proteins; hence systematic comparisons of experiment versus theory have rarely been possible. More efficient methods to acquire and assign SSNMR spectra of entire proteins will permit such analyses and assist in developing a more complete understanding of the differences that sometimes exist between X-ray diffraction and solution NMR structures of proteins.[5]

Thus, in recent years major research efforts have been aimed at developing methods to accelerate the rate of data accumulation and interpretation by SSNMR, principally by studying uniformly-^{13}C,^{15}N-enriched peptides and proteins. In particular, magic-angle spinning (MAS) SSNMR methodology for de novo assignment and structure determination of uniformly-^{13}C,^{15}N-labeled peptides and proteins has rapidly advanced. Landmark high-field (750−800 MHz) MAS studies demonstrated that 2D ^{13}C−^{13}C correlation spectra of basic pancreatic trypsin inhibitor (BPTI)[6] and a 62-residue α-spectrin SH3 domain[7] could be acquired with sub-ppm resolution. Site-resolved signals from these spectra could be identified by residue type and assigned by comparison to solution NMR data. Subsequently, 2D ^{15}N−^{13}C spectra established sequence-specific correlations, critical

(1) Leibmann, C. *Curr. Pharm. Design* **2004**, *10*, 1937−1958.
(2) Caughey, B.; Lansbury, P. T. *Annu. Rev. Neurosci.* **2003**, *26*, 267−298.
(3) McDowell, L. M.; Schaefer, J. *Curr. Opin. Struct. Biol.* **1996**, *6*, 624−629.
(4) Tycko, R. *Prog. Nucl. Magn. Reson. Spectrosc.* **2003**, *42*, 53−68.
(5) Smith, S. O.; Farr-Jones, S.; Griffin, R. G.; Bachovchin, W. W. *Science* **1989**, *244*, 961−964.
(6) McDermott, A.; Polenova, T.; Bockmann, A.; Zilm, K. W.; Paulsen, E. K.; Martin, R. W.; Montelione, G. T. *J. Biomol. NMR* **2000**, *16*, 209−219.
(7) Pauli, J.; van Rossum, B.; Forster, H.; de Groot, H. J. M.; Oschkinat, H. *J. Magn. Reson.* **2000**, *143*, 411−416.

for the complete ^{13}C and ^{15}N assignments of the SH3 domain.[8] To date, MAS spectra of at least four other proteins have been assigned: in one case, microcrystalline ubiquitin signals were assigned by combining high-field (800 MHz) $^{13}C-^{13}C$ data to resolve side-chain resonances[9] with lower-field (400 MHz) 3D $^{15}N-^{13}C-^{13}C$ experiments to correlate the backbone signals;[10] in the other study, a variety of elegant 2D spectra at 500−600 MHz, including *J*-decoupled INADEQUATE methods, were employed to assign the regulatory protein Crh and analyze its secondary structure;[11] in the third, thioredoxin was assigned by differential isotopic labeling of peptide fragments;[12] finally, the scorpion-venom peptide kaliotoxin was assigned, and its structure was determined by an efficient protocol of 2D experiments.[13]

Clearly these studies represent substantial progress for the discipline. Nevertheless, it remains an open question when such techniques will become generally applicable and routine for nonspecialists. The development and popularization of solution NMR protein structure determination techniques over the last two decades benefited greatly from investigation of small globular domains such as BPTI and ubiquitin, with the latter used as the working example for an entire textbook.[14] Likewise, SSNMR studies of these same proteins have been and will continue to be critical for the maturation of the discipline and successful application to unique protein systems, because the detailed study of model proteins is fundamental to the SSNMR technique development. For example, chemical shift assignment techniques developed with model peptides[15,16] and the α-spectrin SH3 protein[8] were subsequently applied to membrane-bound light-harvesting[17] and peptide/G-protein coupled receptor[18] complexes, and several research groups have extensively investigated ubiquitin[9,10,19−27] to develop pulse sequences for application to larger proteins.[28]

Beyond the methodological aspects of such studies, new chemical insights can be directly derived from analyzing correlation spectra of solid proteins. For example, according to atomic resolution crystal structures, many protein residues populate multiple side-chain conformations at cryogenic temperatures.[29,30] Unfortunately, crystallography cannot conclusively differentiate static from dynamic disorder among rotameric states. Direct measurement of protein conformational changes over a range of temperatures could provide a new type of atomic resolution data to enlighten this physical problem. Specifically, MAS NMR spectra yield chemical shifts, line shapes, dipolar scaling factors, and relaxation parameters that can be interpreted in terms of chemistry, including details of secondary structure, hydrogen bonding, and protonation states.

For these reasons, both practical and fundamental, we have investigated the 56-residue β1 immunoglobulin binding domain of protein G (GB1) by acquiring and interpreting a variety of 2D and 3D chemical shift and dipolar correlation spectra. GB1 is an especially well characterized protein, which has been the subject of numerous solution NMR,[31] crystallography,[32] mutagenesis,[33−35] and protein folding[36−39] studies. Therefore we expected that GB1 might serve as an excellent standard for comparing SSNMR to other experimental methods. Here we show that GB1 can be rapidly and reproducibly prepared as a hydrated, microcrystalline precipitate for MAS experiments, yielding spectra with especially high sensitivity and resolution, which enable complete sequential assignments of ^{13}C and ^{15}N chemical shifts at 500 MHz ^{1}H frequency, a relatively modest field strength by today's standards. The GB1 chemical shifts agree remarkably well with solution NMR spectra acquired from the same sample preparation and yield empirical backbone torsion angles in very good agreement with the crystal structure. Therefore GB1 is an excellent platform for the development of pulse sequence and data analysis methodology, sharing some traits with the aforementioned model proteins but also several favorable characteristics that are not available in those systems. For example, GB1 has exceptionally high thermostability (T_m ∼87 °C),[40] despite its lack of disulfide bonds, which allows it to be expressed and purified in much higher yield than proteins that contain disulfides, such as BPTI.[41] In comparison to SH3,[7,8] GB1 contains a significant percentage of α-helical residues, which are useful in evaluating pulse sequence performance and structural parameters in a variety of secondary structure contexts. In comparison to Crh,[11] GB1 is more generally available and has a more extensive body of data available from mutagenesis,

(8) Pauli, J.; Baldus, M.; van Rossum, B.; de Groot, H.; Oschkinat, H. *ChemBioChem* **2001**, *2*, 101−110.
(9) Igumenova, T. I.; McDermott, A. E.; Zilm, K. W.; Martin, R. W.; Paulson, E. K.; Wand, A. J. *J. Am. Chem. Soc.* **2004**, *126*, 6720−6727.
(10) Igumenova, T. I.; Wand, A. J.; McDermott, A. E. *J. Am. Chem. Soc.* **2004**, *126*, 5323−5331.
(11) Bockmann, A.; Lange, A.; Galinier, A.; Luca, S.; Giraud, N.; Juy, M.; Heise, H.; Montserret, R.; Penin, F.; Baldus, M. *J. Biomol. NMR* **2003**, *27*, 323−339.
(12) Marulanda, D.; Tasayco, M. L.; McDermott, A.; Cataldi, M.; Arriaran, V.; Polenova, T. *J. Am. Chem. Soc.* **2004**, *126*, 16608−16620.
(13) Lange, A.; Becker, S.; Seidel, K.; Giller, K.; Pongs, O.; Baldus, M. *Angew. Chem., Int. Ed.* **2005**, *44*, 2089−2092.
(14) Cavanagh, J.; Fairbrother, W. J.; Palmer, A. G.; Skelton, N. J. *Protein NMR Spectroscopy: Principles and Practice*; Academic Press: San Diego, 1996.
(15) Baldus, M.; Geurts, D. G.; Hediger, S.; Meier, B. H. *J. Magn. Reson. A* **1996**, *118*, 140−144.
(16) Baldus, M.; Petkova, A. T.; Herzfeld, J. H.; Griffin, R. G. *Mol. Phys.* **1998**, *95*, 1197−1207.
(17) Egorova-Zachernyuk, T. A.; Hollander, J.; Fraser, N.; Gast, P.; Hoff, A. J.; Cogdell, R.; de Groot, H. J. M.; Baldus, M. *J. Biomol. NMR* **2001**, *19*, 243−253.
(18) Luca, S.; White, J. F.; Sohal, A. K.; Filippov, D. V.; van Boom, J. H.; Grisshammer, R.; Baldus, M. *Proc. Natl. Acad. Sci. U.S.A.* **2003**, *100*, 10706−10711.
(19) Hong, M. *J. Biomol. NMR* **1999**, *15*, 1−14.
(20) Hong, M. *J. Magn. Reson.* **1999**, *139*, 389−401.
(21) Hong, M. *J. Am. Chem. Soc.* **2000**, *122*, 3762−3770.
(22) Lange, A.; Luca, S.; Baldus, M. *J. Am. Chem. Soc.* **2002**, *124*, 9704−9705.
(23) Paulson, E. K.; Morcombe, C. R.; Gaponenko, V.; Dancheck, B.; Byrd, R. A.; Zilm, K. W. *J. Am. Chem. Soc.* **2003**, *125*, 15831−15836.
(24) Morcombe, C. R.; Gaponenko, V.; Byrd, R. A.; Zilm, K. W. *J. Am. Chem. Soc.* **2004**, *126*, 7196−7197.
(25) Sonnenberg, L.; Luca, S.; Baldus, M. *J. Magn. Reson.* **2004**, *166*, 100−110.
(26) Morcombe, C. R.; Gaponenko, V.; Byrd, R. A.; Zilm, K. W. *J. Am. Chem. Soc.* **2005**, *127*, 397−404.
(27) Zech, S. G.; Wand, A. J.; McDermott, A. E. *J. Am. Chem. Soc.* **2005**, *127*, 8618−8626.
(28) McDermott, A. E. *Curr. Opin. Struct. Biol.* **2004**, *14*, 554−561.
(29) MacArthur, M. W.; Thornton, J. M. *Acta Crystallogr., Sect. D* **1999**, *55*, 994−1004.
(30) Chakrabarti, P.; Pal, D. *Prog. Biophys. Mol. Biol.* **2001**, *76*, 1−102.
(31) Gronenborn, A. M.; Filpula, D. R.; Essig, N. Z.; Achari, A.; Whitlow, M.; Wingfield, P. T.; Clore, G. M. *Science* **1991**, *253*, 657−661.
(32) Gallagher, T.; Alexander, P.; Bryan, P.; Gilliland, G. L. *Biochemistry* **1994**, *33*, 4721−4729.
(33) Frank, M. K.; Dyda, F.; Dobrodumov, A.; Gronenborn, A. M. *Nat. Struct. Biol.* **2002**, *9*, 877−885.
(34) Byeon, I. J. L.; Louis, J. M.; Gronenborn, A. M. *J. Mol. Biol.* **2003**, *333*, 141−152.
(35) Ramirez-Alvarado, M.; Cocco, M. J.; Regan, L. *Protein Sci.* **2003**, *12*, 567−576.
(36) Kuszewski, J.; Clore, G. M.; Gronenborn, A. M. *Protein Sci.* **1994**, *3*, 1945−1952.
(37) Frank, M. K.; Clore, G. M.; Gronenborn, A. M. *Protein Sci.* **1995**, *4*, 2605−2615.
(38) Sheinerman, F. B.; Brooks, C. L. *Proc. Natl. Acad. Sci. U.S.A.* **1998**, *95*, 1562−1567.
(39) Ding, K. Y.; Louis, J. M.; Gronenborn, A. M. *J. Mol. Biol.* **2004**, *335*, 1299−1307.
(40) Alexander, P.; Orban, J.; Bryan, P. *Biochemistry* **1992**, *31*, 7243−7248.
(41) Castro, M. J. M.; Anderson, S. *Biochemistry* **1996**, *35*, 11435−11446.

solution NMR, and other biophysical techniques. In comparison to ubiquitin, GB1 is more thermostable and yields spectra of higher sensitivity and resolution on the same NMR instruments (included in the Supporting Information), due to the fact that it packs in the crystal lattice with especially high density.

A final novel feature of GB1, which we believe is unique so far among proteins studied by SSNMR methods, is that near room temperature (280 K) all ^{13}C and ^{15}N signals are observed with high resolution and sensitivity, including the terminal amino and carboxyl resonances, side-chains, loops, and turns. To our knowledge, in all other proteins subsets of these signals are not observed, due presumably to conformational exchange events with rate constants in the intermediate (microsecond) regime. We demonstrate in GB1 that sensitivity and resolution degrade markedly as the temperature is lowered to ~210−220 K but recover as the temperature is lowered further (<200 K). Near the transition temperature, signal intensities are systematically attenuated among all residues, but most among residues at the surface of the protein, involved in intermolecular contacts and/or exposed to solvent in the crystal lattice. It has been shown previously that strong correlations between protein ^{15}N and solvent ^{1}H resonances can be observed in SSNMR spectra, to identify bound water molecules.[42] Here we complement this idea by showing that the signal intensity variations among ^{13}C and ^{15}N sites as a function of residue position identify dynamic regions of proteins and interactions with solvent. In this study, we present direct insight into these site-specific effects with chemical shift and dipolar spectra and establish GB1 as a platform for novel studies of protein structure and dynamics in the solid state.

Experimental Section

The T2Q mutant of GB1 was employed, produced from a cDNA construct kindly provided by A. M. Gronenborn (National Institutes of Health). This mutation reduces the cleavage of the N-terminal Met residue[43] but has minimal effect upon the structure, as determined by fingerprint solution NMR spectra and behavior in protein folding and dynamics studies.[43,44] Bacterial expression using minimal media (1 g/L $^{15}NH_4Cl$, 2 g/L ^{13}C glucose) with a supplementary dose (10 mL of 10x) of BioExpress rich media (Cambridge Isotope Laboratories)[45] typically yielded 100 mg protein per L of media; protein expression was induced with 500 μM isopropyl β-D-thiogalactoside for 4 h. The cell pellet was disrupted by heating to 80 °C for 5 min in phosphate-buffered saline (200 mM NaCl, 50 mM KH_2PO_4/K_2HPO_4, pH 7). The supernatant from this initial purification step contained GB1 at ~85−90% purity, as determined by SDS−PAGE and solution NMR. Gel exclusion chromatography (Sephadex 100) with 100 mM NaCl, 50 mM phosphate buffer (pH 7) was performed as the final purification step. Peak fractions were pooled and concentrated with Centriplus 3 kDa MWCO filters, and the buffer thoroughly exchanged to 50 mM sodium phosphate, pH 5.5.

Many of the spectra presented here were obtained from a single purified sample (~45 mg GB1 in 1.5 mL buffer). Approximately a third of this material (500 μL, ~3 mM protein concentration, 50 mM phosphate, pH 5.5, 0.1 mM DSS) was utilized for collection of standard solution NMR $^{1}H-^{15}N$ HSQC, $^{1}H-^{13}C$ HSQC, HNCACB, HNCO, and HNCOCA experiments. Although these experiments have been previously performed on GB1, we wished to confirm the published assignments under very similar conditions to the SSNMR sample; the solution NMR chemical shifts reported here were derived from these spectra at 293 K. Solution NMR experiments were performed on a 600 MHz Varian UnityINOVA triple resonance spectrometer with a 5-mm triaxial gradient HCN probe, using the BioPack interface in VNMR Version 6.1D (Varian, Inc., Palo Alto, California).

A second fraction of the $^{15}N,^{13}C$ sample was precipitated and packed into a 3.2 mm (22 μL) rotor (Varian, Inc.) for SSNMR studies. The precipitation conditions were determined by the hanging drop vapor diffusion method, starting with the single crystal (orthorhombic) condition reported by Gallagher et al.[32] We employed a slightly higher pH and different salt in order to make the most accurate comparison with the solution NMR spectra. The total mass of material packed into the rotor was 15−16 mg, of which ~10 mg was protein (i.e., ~60−70% concentration by mass, determined by long pulse-delay ^{13}C Bloch decay experiments in comparison to sensitivity standards), which is unusually high for a protein but consistent with the reported solvent content of ~26% for the orthorhombic crystal form.[32] (Additional details are included in the Supporting Information.)

MAS SSNMR experiments were performed on a 500 MHz Varian InfinityPlus four-channel spectrometer, with T3 $^{1}H-^{13}C-^{2}H-^{15}N$ and Balun $^{1}H-^{13}C-^{15}N$ 3.2 mm MAS probes. Unless otherwise noted, the MAS rate was 11.111 kHz, and the temperature of variable temperature gas set to 273 K with 100 scfh flow, resulting in an effective mean sample temperature (due to frictional heating and geometrical offset factors) of 280 ± 4 K, by methanol calibration.[46] Pulse sequences were implemented with tangent ramped cross polarization[47] at ~60−70 kHz and TPPM ^{1}H decoupling at ~70−75 kHz.[48] Pulse widths ($\pi/2$) on ^{1}H, ^{13}C, and ^{15}N were typically 2.0, 3.0, and 5.0 μs. Additional pulse sequence details are included in the respective figure captions.

Data were processed with nmrPipe,[49] employing Lorentzian-to-Gaussian apodization, zero filling to all dimensions prior to Fourier transformation, and polynominal baseline (frequency-domain) correction to the direct dimension. Additional acquisition and processing parameters for each spectrum are provided in the respective figure captions. Chemical shifts were referenced according to Morcombe and Zilm, using the DSS scale[50] with adamantane as a secondary standard, assuming its downfield signal to resonate at 40.48 ppm; reproducibility of the measurements from one sample to the next, by adamantane reference spectra before and after protein experiments, was ±0.02 ppm. Spectral peak picking and assignments were performed with Sparky version 3 (T. D. Goddard and D. G. Kneller, University of California, San Francisco).

Results and Discussion

a. Sample Preparation and Spectral Resolution. High-resolution SSNMR spectra of a crystalline protein were first acquired by Torchia and co-workers,[51] and several recent studies have shown that the details of sample precipitation and/or crystallization dramatically impact the resolution of 2D and 3D SSNMR spectra.[7,10,11] This methodology has been formalized by Martin and Zilm, in a study which demonstrated in several proteins that sample precipitation conditions determined from hanging drop vapor diffusion screens translate well to batch quantities to yield especially high-quality MAS spectra.[52]

(42) Paulson, E. K.; Morcombe, C. R.; Gaponenko, V.; Dancheck, B.; Byrd, R. A.; Zilm, K. W. *J. Am. Chem. Soc.* **2003**, *125*, 14222−14223.
(43) Smith, C. K.; Withka, J. M.; Regan, L. *Biochemistry* **1994**, *33*, 5510−5517.
(44) Goehlert, V. A.; Krupinska, E.; Regan, L.; Stone, M. J. *Protein Sci.* **2004**, *13*, 3322−3330.
(45) Holdeman, T. C.; Gardner, K. H. *J. Biomol. NMR* **2001**, *21*, 383−384.
(46) Van Geet, A. L. *Anal. Chem.* **1968**, *42*, 2227.
(47) Hediger, S.; Meier, B. H.; Kurur, N. D.; Bodenhausen, G.; Ernst, R. R. *Chem. Phys. Lett.* **1994**, *223*, 283−288.
(48) Bennett, A. E.; Rienstra, C. M.; Auger, M.; Lakshmi, K. V.; Griffin, R. G. *J. Chem. Phys.* **1995**, *103*, 6951−6958.
(49) Delaglio, F.; Grzesiek, S.; Vuister, G. W.; Zhu, G.; Pfeifer, J.; Bax, A. *J. Biomol. NMR* **1995**, *6*, 277−293.
(50) Morcombe, C. R.; Zilm, K. W. *J. Magn. Reson.* **2003**, *162*, 479−486.
(51) Cole, H. B.; Sparks, S. W.; Torchia, D. A. *Proc. Natl. Acad. Sci. U.S.A.* **1988**, *85*, 6362−6365.
(52) Martin, R. W.; Zilm, K. W. *J. Magn. Reson.* **2003**, *165*, 162−174.

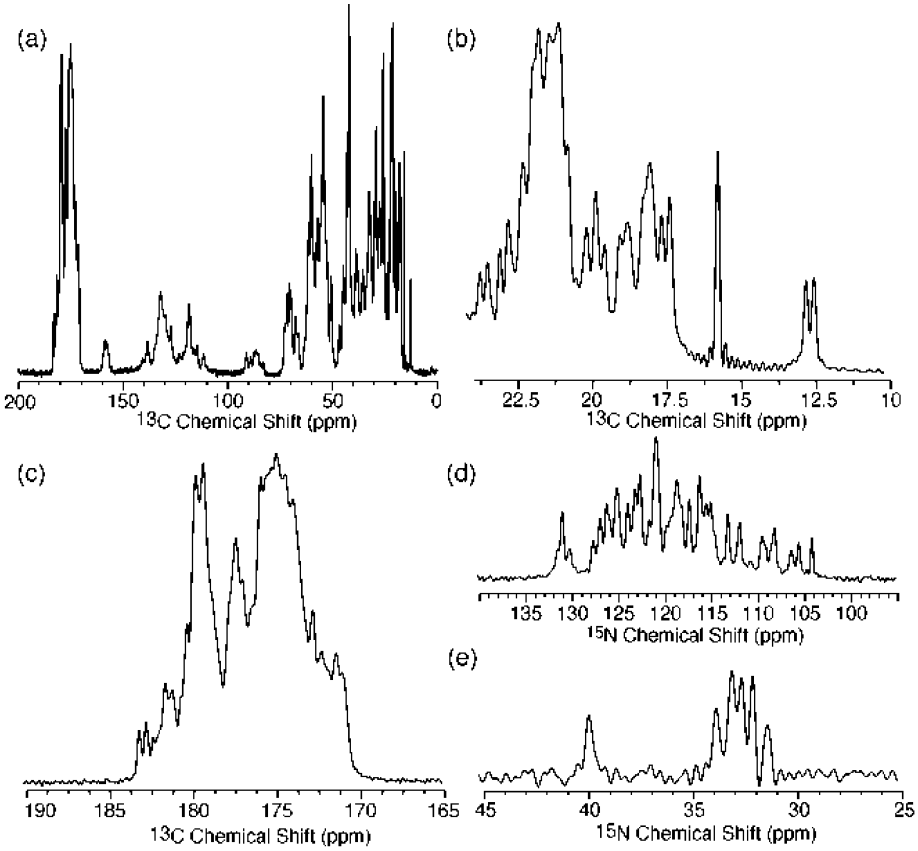

Figure 1. CP-MAS 1D ^{13}C and ^{15}N spectra of microcrystalline GB1, ~10 mg in a 3.2 mm (22 μL) Varian rotor, 11.111 kHz MAS rate. (a) Full ^{13}C bandwidth, 2 ms $^{1}H-^{13}C$ CP contact time (tangent ramp on ^{13}C), 38.4 ms (2560 × 15 μs) acquisition time, 70 kHz ^{1}H TPPM decoupling (7.1 μs, 18°),[48] 128 scans, 2 s pulse delay. (b) Upfield region of spectrum (a), illustrating fine structure among methyl ^{13}C signals in many resonances including the Ile Cδ1 at 12.8 ppm and a singlet (Met Cϵ) at 15.9 ppm. (c) Carbonyl region of the ^{13}C spectrum. The furthest downfield resonance is a Glu Cδ. (d) Amide region of ^{15}N 1D spectrum, 2 ms $^{1}H-^{15}N$ contact time (tangent ramp on ^{15}N), 46 ms (768 × 60 μs) acquisition time, 256 scans, 65 kHz ^{1}H TPPM decoupling (7.6 μs, 14°). (e) Amino region of the same ^{15}N 1D spectrum.

By following this procedure for GB1, especially high-resolution spectra were observed, including fine structure due to homonuclear scalar couplings between ^{13}C nuclei in several resonances, such as the outlying carboxylate and methyl signals (Figure 1b and 1c). The expansion (Figure 1b) of the methyl region illustrates a one-bond scalar coupling (34 ± 1 Hz) splitting the peak at 12.8 ppm (later assigned as Ile6 Cδ1) more than halfway to the baseline; the individual components of the doublet have line widths (full width at half-maximum, fwhm) of 16−20 Hz (0.12−0.16 ppm). We attribute the remaining line width to (a) two-bond scalar couplings (Cδ1−Cβ and Cδ1−Cγ2, a few Hz each), (b) B_0 inhomogeneity (with this probe, adamantane ^{13}C line widths were 5 ± 1 Hz fwhm), (c) imperfect heteronuclear $^{1}H-^{13}C$ decoupling, and (d) sample heterogeneities. For example, the singlet at 15.9 ppm (M1 Cϵ) is narrower (a fwhm line width of 15 Hz) because it lacks a one-bond scalar coupling and has only one two-bond coupling. The downfield doublet at 183.2 ppm (Figure 1c, E56 Cδ) is split by a 52 ± 1 Hz Cγ−Cδ scalar coupling; the individual components are 30 ± 3 Hz. In the ^{15}N spectrum line widths are typically 0.3 to 0.5 ppm, dominated by the $^{13}C-^{15}N$ scalar interactions, which were not decoupled in this set of experiments. Throughout the ^{13}C and ^{15}N 1D spectra, resolution is consistent with a nano- or microcrystalline sample preparation exhibiting heterogeneities of significantly less than 0.1 ppm, with essentially instrument-limited resolution. We believe that this represents a new benchmark for spectral resolution in solid proteins. (A direct comparison with ubiquitin is included in the Supporting Information.) To determine the optimal temperature for performing chemical shift assignments, we explored the range from ~280 to ~220 K and found that as temperatures were lowered over this range, resolution significantly deteriorated. Therefore we chose to perform the ^{13}C and ^{15}N assignments near room temperature and subsequently to explore the temperature-dependence in greater detail. Under these experimental conditions at 500 MHz, GB1 is stable for several months.

b. Chemical Shift Assignments. Following assignment procedures established by solution NMR[53] and recent SSNMR studies,[6,7,9,11] we focus discussion here on the unique features of GB1 that enabled assignments to be performed at the relatively low B_0 field strength of 11.7 T (500 MHz ^{1}H frequency). Ile and Met each occur only once in GB1, and with characteristic chemical shifts and multiplicities; Ala, Thr, Val and Leu spin systems were identified by side-chain chemical shift patterns, Gly by its distinctive Cα−C′ correlations, the aromatics based on Cγ and Cδ shifts, and the Asx and Glx residues based on side-chain carbonyls or carboxyls. Pro, His, Cys and Ser are not present in GB1. Lys residues were difficult to categorize with confidence from the $^{13}C-^{13}C$ 2D, but were identified in the $^{15}N-^{13}C-^{13}C$ spectra.

(53) Wüthrich, K. *NMR of Proteins and Nucleic Acids*; John Wiley and Sons: New York, 1986.

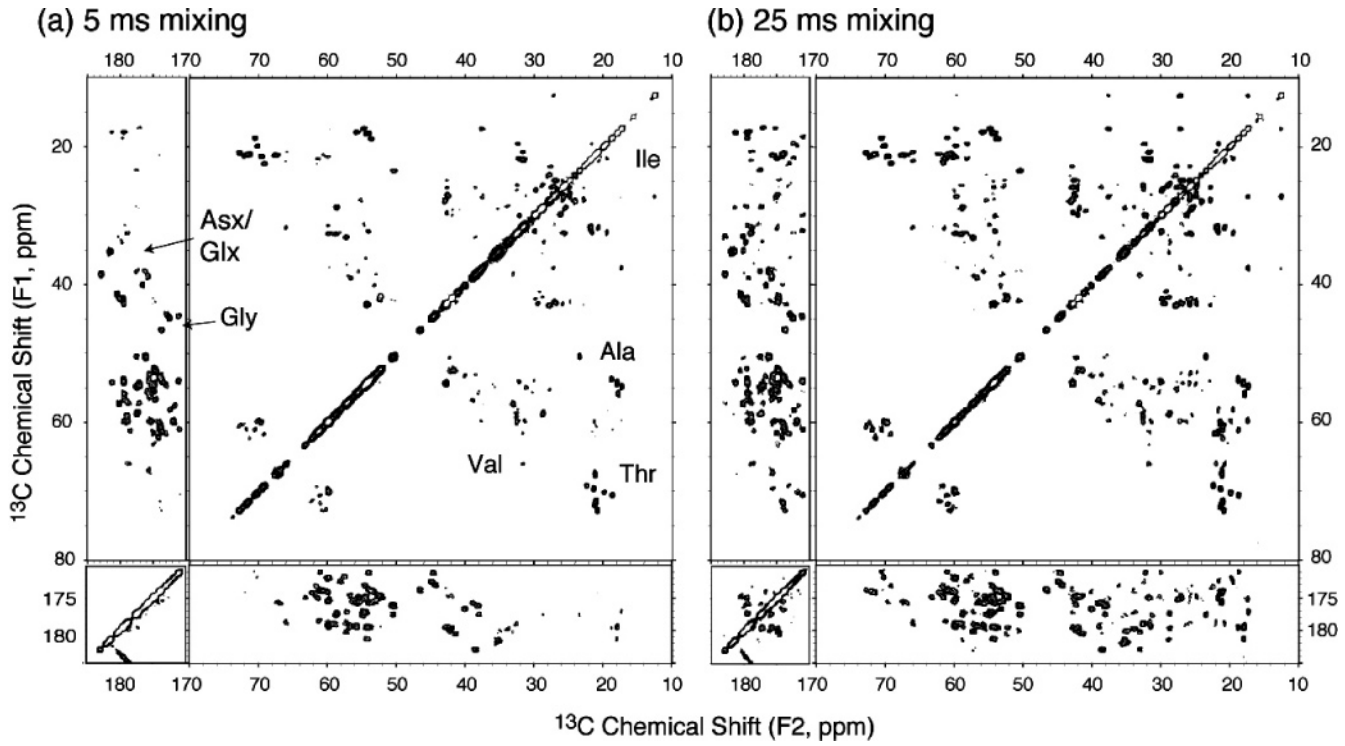

Figure 2. 2D $^{13}C-^{13}C$ spectra of GB1. (a) 5 ms DARR mixing[54] (also known as RAD[24,55]) (b) 25 ms mixing. In both cases, the raw data set size was 1280 rows with a 16.5 μs dwell time in t_1 (TPPI),[56] and 2560 complex points with a 15 μs dwell time in t_2. A rotary resonant ^{1}H field ($n = 1$, 11.1 kHz) was applied during the DARR mixing period. Four scans were acquired per row, with a pulse delay of 2 s, resulting in a total measurement time of 3.0 h. Data were processed with 15 Hz net line broadening (Lorentzian-to-Gaussian apodization) and zero filling to 2048 (F1) $\times$ 8192 (F2) complex points.

The 2D $^{13}C-^{13}C$ spectra employing DARR[54] (RAD)[24,55] mixing produced some uncertainties arising from (a) variations in peak intensity as a function of side-chain topology and (b) additional cross-peaks arising from two-step dipolar transfers. We compared DARR at several mixing times ranging from 2.5 to 50 ms, with the 5 and 25 ms mixing times shown here (Figure 2). At 5 ms mixing, predominantly one-bond correlations are observed, along with some weak two-bond correlations (e.g., Ala C′−Cβ, Thr Cα−Cγ); at 25 ms mixing, stronger two- and three-bond correlations are observed. Although we found the total information content of DARR spectra to be greater than any other individual 2D $^{13}C-^{13}C$ experiment, a consequence of the multistep transfers is that cross-peak intensities among residue types, e.g., in the Cα−Cβ region, may vary considerably. In particular, branched-chain carbons retain a relatively small percentage of the total intensity; e.g., the Val Cα-Cβ cross-peaks are several times weaker than the Ala Cα−Cβ. Some strong two-bond correlations may appear with greater intensity than the weaker one-bond correlations, even at short (5 ms) mixing times. This can complicate the identification of spin systems in congested spectral regions. For example, Val residues with downfield shifted Cα signals (e.g., V29) give rise to Cα−Cγ cross-peaks in close proximity to the Thr Cβ−Cγ peaks ($\sim$58, $\sim$21 ppm). Residues including Met, Leu, Ile, and Gln/Glu have Cγ shifts in the range 28−35 ppm, in the same region of the Cβ shifts of Val and Lys. Similar complications arise in the ($\sim$174, $\sim$43 ppm) region of the spectrum, where Leu and Asp C′−Cβ peaks are in close proximity to Gly C′−Cα peaks. In our spectra the Gly signals have strong intensities, so confusion with a C′−Cβ peak is unlikely; however, Igumenova et al. have reported that the Gly signals in ubiquitin have highly variable intensities (with some missing entirely),[10] in which case the difficulties in distinguishing between these signals from competing C′−Cβ resonances would be exacerbated. Asn and Asp C′−Cβ peaks may obscure Asn Cγ−Cβ peaks near 176, 38 ppm; Asn C′−Cβ peaks appear near Asp Cγ−Cβ peaks at $\sim$180, 42 ppm, and similar effects are apparent in the Gln and Glu Cδ−Cγ region. Conversely, the two-step transfers that give rise to Asp and Asn Cγ−Cα peaks may hinder analysis of the C′−Cα region of the spectrum. These issues arise also with RFDR mixing,[57] because the recoupling Hamiltonian inherently depends on chemical shift differences, giving rise to stronger peak intensities near rotational resonance conditions.[58]

The residue type identification was completed with a complementary 2D $^{13}C-^{13}C$ spectrum with SPC-5_3 double quantum mixing. We chose a mixing time of 1.08 ms (12 rotor periods, or two full supercycles of the SPC-5_3 sequence) to ensure only one-bond transfer.[59,60] Transfer efficiencies for Cα−Cβ and Cα−C′ under these SPC-5_3 conditions were typically 25−30% of the initial (diagonal) peak intensity. Figure 3 compares the relevant regions of the spectra for SPC-5_3 and DARR mixing. In the Cα−Cβ region of the SPC-5_3 spectrum ($\sim$50−65 ppm,

(54) Takegoshi, K.; Nakamura, S.; Terao, T. *Chem. Phys. Lett.* **2001**, *344*, 631−637.
(55) Zilm, K. W. Oral Presentation at the 40th Experimental NMR Conference, Orlando, FL, 1999.
(56) Marion, D.; Wuthrich, K. *Biochem. Biophys. Res. Commun.* **1983**, *113*, 967−974.
(57) Bennett, A. E.; Ok, J. H.; Griffin, R. G.; Vega, S. *J. Chem. Phys.* **1992**, *96*, 8624−8627.
(58) Raleigh, D. P.; Levitt, M. H.; Griffin, R. G. *Chem. Phys. Lett.* **1988**, *146*, 71−76.
(59) Hohwy, M.; Rienstra, C. M.; Jaroniec, C. P.; Griffin, R. G. *J. Chem. Phys.* **1999**, *110*, 7983−7992.
(60) Hohwy, M.; Rienstra, C. M.; Griffin, R. G. *J. Chem. Phys.* **2002**, *117*, 4973−4987.

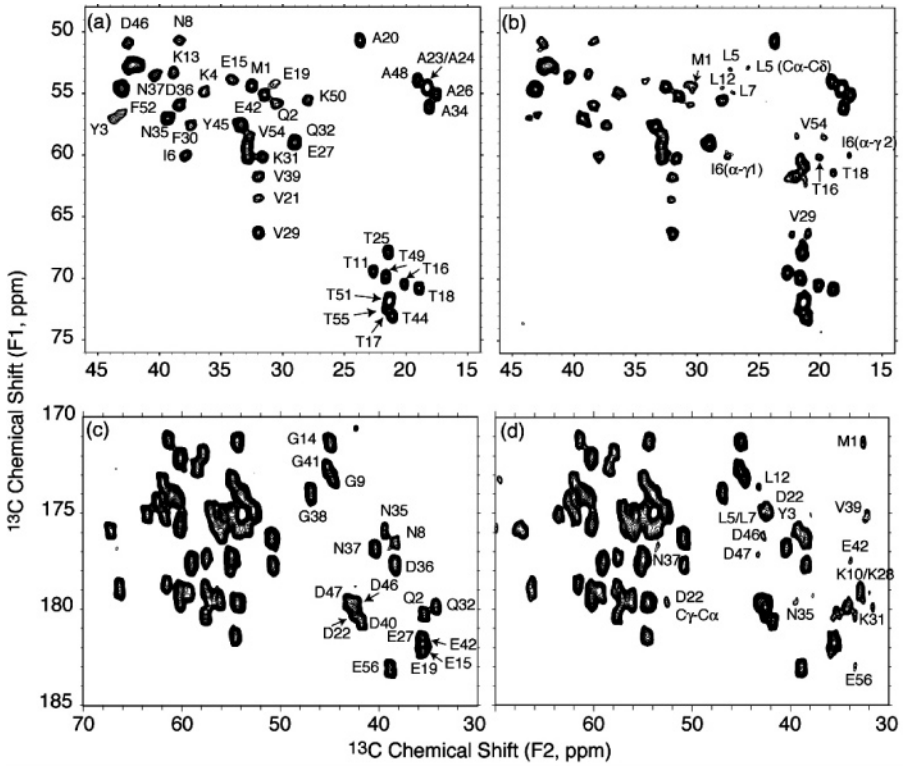

Figure 3. 2D $^{13}C-^{13}C$ spectra comparing SPC-5_3 and DARR mixing schemes (500 MHz ^1H frequency). (a) SPC-5_3, aliphatic region. Cross-peaks arise only from one-bond transfers, primarily C$\alpha-$Cβ (or C$\beta-$Cγ for the Thr resonances in the lower right corner). Mixing time was 1.08 ms, with a 37 kHz field on ^{13}C and 105 kHz ^1H decoupling. (b) Aliphatic region of $^{13}C-^{13}C$ 2D with DARR mixing (5 ms, same data set shown in Figure 2(a)). The additional peaks labeled are C$\alpha-$Cγ correlations, resulting from two-step dipolar transfers, and in one case a C$\alpha-$Cδ correlation (L5) from a three-step transfer. (c) Carbonyl-aliphatic region of SPC-5_3 spectrum. One-bond cross-peaks are labeled in the right half of the spectrum (Gly C$'-$Cα, Asn/Asp C$\gamma-$Cβ, Gln/Glu C$\delta-$Cγ). (d) Carbonyl-aliphatic region of the DARR spectrum. The added labels correspond to sites two bonds apart (primarily C$'-$Cβ). Peaks are labeled site-specifically, based on sequential assignments determined from the heteronuclear spectra described below. In all portions of this figure the contour levels have been drawn starting at 12.5% (a, b) or 10% (c, d) of the intensity of the strongest peak in this region of the spectrum, to permit direct comparison of relative peak intensities.

$\sim$25$-$45 ppm), the variations in intensity are reduced somewhat in comparison to DARR. However, some variations are still evident, for reasons to be considered in more detail below.

The complementary information in the DARR and SPC-5_3 data sets was particularly important for unambiguously assigning the region of the 2D spectrum containing side-chain carbonyl resonances, because the initial DARR buildup rate is fast for C$'-$Cα pairs near rotational resonance (at this spinning rate of 11.111 kHz, corresponding to 88.9 ppm at the ^{13}C frequency) but slower for the side-chain carbonyls coupled to methylene signals in the 30$-$40 ppm range. During the 5 ms mixing time, C$'-$Cβ resonances in the DARR spectrum (e.g., Asp, Val, and Lys) are close to the Asp/Asn C$\beta-$Cγ and Glu/Gln C$\gamma-$Cδ resonances. In the SPC-5_3 spectrum, the polarization transfer efficiency does not significantly depend on chemical shift differences. The SPC-5_3 spectrum alone was not adequate to assign all the spin systems uniquely but served as an effective complement to the DARR spectra to distinguish between one- and two-step polarization transfers.

With amino acid type identification and side-chain correlations established, heteronuclear correlations along the peptide backbone were derived from relayed $^{15}N-(^{13}C)-^{13}C$ 2D spectra,[8,61] based on band-selective SPECIFIC $^{15}N-^{13}C$ CP[16] and DARR $^{13}C-^{13}C$ mixing.[54] The resolution of the indirect ^{15}N dimension distinguished most residues, and the sensitivity enabled observation of cross-peaks arising from polarization transfer (by DARR) over two or more $^{13}C-^{13}C$ bonds. The Cα represents a bifurcation point in the ^{13}C polarization transfer pathway, so the DARR mixing time was set to 5 ms; for all Cα sites, correlations to C$'$ and Cβ resonances were also observed, along with many Cγ signals. For the N$-$C$'-$CX, a longer (15 ms) period was employed to drive a larger percentage of the polarization to Cβ and Cγ resonances. In this context, the low signal loss during DARR mixing was favorable. The two spectra in Figure 4 (N$-$C$\alpha-$CX and N$-$C$'-$CX, following the notation of previous authors[8,10$-$12] but modified to be consistent with the IUPAC naming conventions[62]) were acquired consecutively in $\sim$2.5 h each, permitting an analysis of superimposed spectra with very high ($\pm$0.1 ppm) precision. We established sequential connectivities starting with the outlying ^{15}N chemical shifts and proceeded in a manner similar to the studies cited above. (Additional details are provided in the Supporting Information.)

The aromatic residues in GB1 have a special significance in the experiments discussed further below, and so we confirmed assignments of these signals by acquiring N$-$C$\alpha-$CX and N$-$C$'-$CX 2D data sets with longer (50 ms) DARR $^{13}C-^{13}C$ mixing times (Figure 5). The line widths in strongly coupled aromatic spin systems (in the absence of local molecular motion) are $>$1 ppm at 500 MHz ^1H frequency; proportional increases in line broadening applied in the data processing enabled us to

(61) Baldus, M. *Prog. Nucl. Magn. Reson. Spectrosc.* **2002**, *41*, 1$-$47.

(62) Markley, J. L.; Bax, A.; Arata, Y.; Hilbers, C. W.; Kaptein, R.; Sykes, B. D.; Wright, P. E.; Wuthrich, K. *Pure Appl. Chem.* **1998**, *70*, 117$-$142.

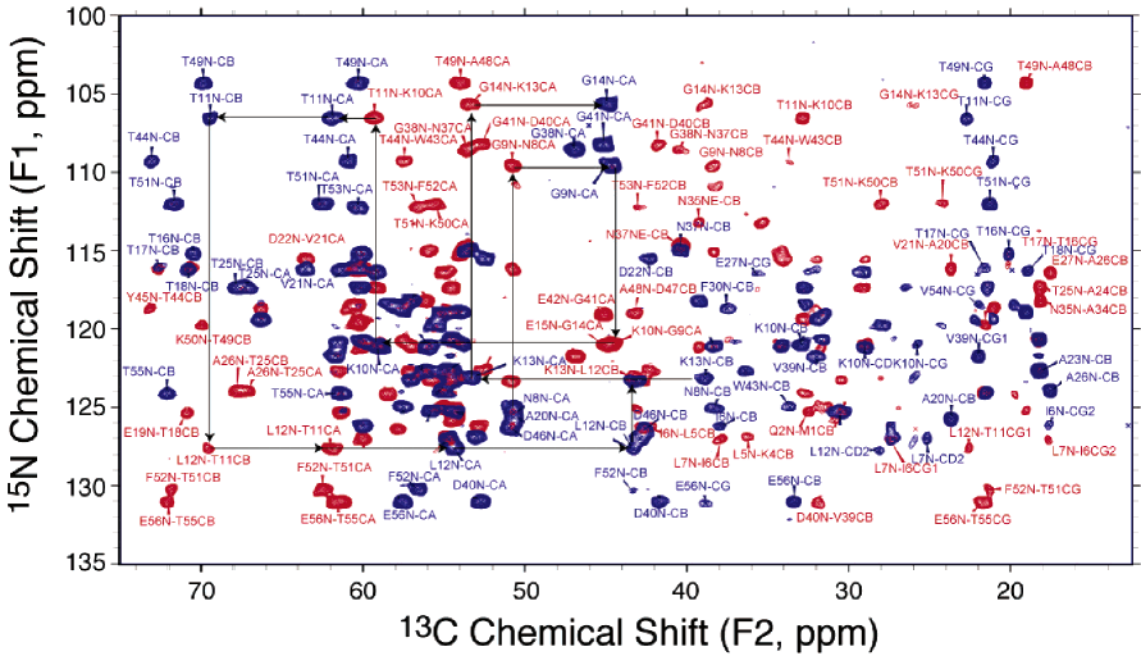

Figure 4. Overlaid $^{15}N-(^{13}C')-^{13}CX$ (red) and $^{15}N-(^{13}C\alpha)-^{13}CX$ (blue) 2D spectra of GB1.[8] Each spectrum was acquired with 1024 rows in the t_1 (^{15}N) dimension with a 22.5 μs dwell time, 4 scans per row, 2 s pulse delay, 2.3 h measurement time. The $^1H-^{15}N$ CP was achieved by matching to the $n = 1$ sideband (^1H field 60 kHz, ^{15}N field 50 kHz with a tangent ramp of ± 6 kHz; 1 ms contact time). In $^{15}N-^{13}C\alpha$ based experiment, the SPECIFIC CP condition[16] was matched for 8 ms by applying a ^{15}N field ($\omega_N/2\pi$) of ~27 kHz ($5/2\ \omega_r/2\pi$) and a ^{13}C field of ~16 kHz ($3/2\ \omega_r/2\pi$), with a tangent ramp of ± 1.5 kHz (ramping down in field amplitude).[63] The ^{13}C carrier was placed at ~40 ppm and the $^{13}C-^{13}C$ DARR mixing time was 5 ms. In the $^{15}N-^{13}C'$ based experiment, the $\omega_N = {}^3/_2\ \omega_r$, $\omega_C = {}^5/_2\ \omega_r$ (at ~172 ppm) SPECIFIC CP condition was used (8 ms contact time), and the DARR mixing time was 15 ms. Net Gaussian line broadenings of 5 and 30 Hz were applied to ^{15}N and ^{13}C, respectively.

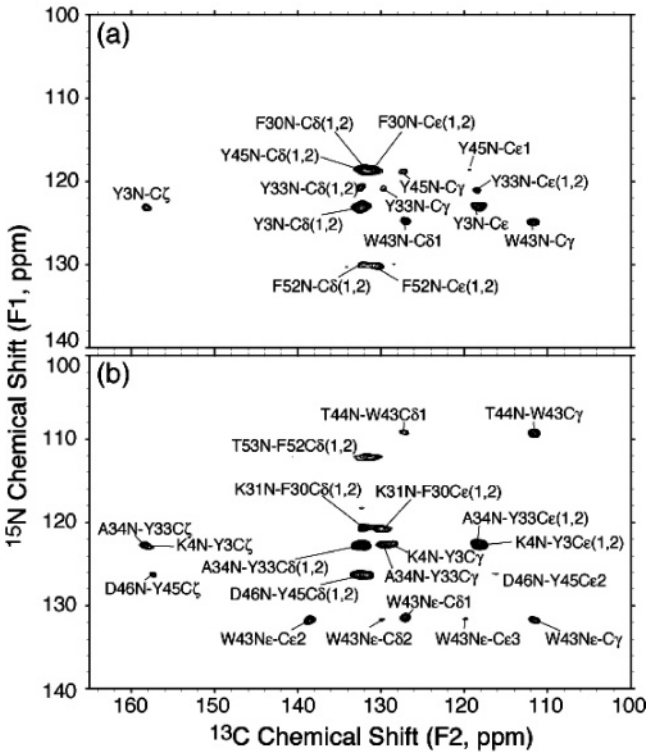

Figure 5. (a) $^{15}N-^{13}C\alpha-^{13}CX$ and (b) $^{15}N-^{13}C'-^{13}CX$ 2D spectra with 50 ms $^{13}C-^{13}C$ mixing time to emphasize aromatic correlations. With the exception of the mixing time, data acquisition parameters were the same for the spectra shown in Figure 4. A larger net line broadening (100 Hz) was applied to the ^{13}C dimension to emphasize the broad aromatic signals.

identify all of the Tyr, Phe, and Trp residues. Although the ^{13}C dimension was not especially well resolved, it was possible to identify all of the ^{15}N signals within or following aromatic residues, including the indole $^{15}N\epsilon$ of W43 in the $N-C'-CX$ spectrum; this signal and the lack of correlations to the $^{15}N\epsilon$ in the $N-C\alpha-CX$ spectra, illustrate a generally useful method for identifying Trp residues in proteins. It is notable that, at this 50 ms mixing time, several correlations to the Tyr $^{13}C\zeta$ signals from the backbone ^{15}N sites are observed; this corresponds to correlation between atoms separated by six ($N-C\alpha-CX$) or seven ($N-C'-CX$) bonds, albeit by sequential stepwise one-bond dipolar transfers; the Y45 and Y33 signals are stronger in the $N-C'-CX$ experiment despite the larger number of intervening bonds, because of the $N-C'$ transfer efficiency is ~50−55%, whereas the $N-C\alpha$ is only ~35−40%. Additional $^{13}C-^{13}C$ 2D spectra with DARR and DREAM mixing[63] were utilized to assign all ^{13}C sites within the aromatic rings.

Overall, in the 2D spectra, approximately 75% of the residues could be assigned in a sequence-specific manner. Some ambiguity remained due to the congestion of seven $^{15}N[i]-^{13}C\alpha[i]$ correlations in the region (122−124 ppm ^{15}N, 53−57 ppm $^{13}C\alpha$) and several additional ^{15}N signals between 120 and 121.5 ppm. Although some of the $^{13}C\beta$ and/or $^{13}C\gamma$ signals broke the degeneracy in this region of the spectrum, the 2D spectra alone were not sufficient to complete the assignments. 3D NCC spectra were therefore utilized to complete the assignments and clarify ambiguities (presented in the Supporting Information).

The heteronuclear 2D spectra exhibited substantial differences in peak intensities, some of which among different residue types can be attributed to the effect of chemical shifts on DARR efficiency and the differences in side-chain dipolar coupling topology. In addition, *within* residue types we found significant

(63) Detken, A.; Hardy, E. H.; Ernst, M.; Kainosho, M.; Kawakami, T.; Aimoto, S.; Meier, B. H. *J. Biomol. NMR* **2001**, *20*, 203−221.

variations. For example, among the intraresidue Ala $^{15}N-^{13}C\beta$ signals, there was a 13% standard deviation relative to the mean intensity (with signal-to-noise ratios of 40−60); the Gly $^{15}N-^{13}C\alpha$ had a 18% normalized standard deviation (again several-fold higher than expected due to noise), and the Thr $^{15}N-^{13}C\beta$ signals showed an especially large variation: among the nine Thr residues (11, 16, 17, 18, 25, 44, 49, 51, and 55) above the noise threshold, the signals varied by a factor of 3.5 (with T49 the strongest, and T17 the weakest), with a standard deviation equal to the mean intensity. Furthermore, the T53 $^{15}N-^{13}C\beta$ signal was not visible above the noise threshold in this experiment (although it could be assigned in the $^{13}C-^{13}C$ 2D spectra by correlations to the $^{13}C\alpha$ and $^{13}C\gamma$). The total integrated intensity of all ^{13}C peaks correlated to each ^{15}N signal followed these trends. The potential sources of signal intensity variations will be considered in further detail below, in the context of dynamics measurements.

The complete ^{13}C and ^{15}N assignments of GB1 are presented in Table 1. To assess the relative ease of assignment, we compared the dispersion of chemical shifts by secondary structure type. In the β-strand regions, ^{15}N, $^{13}C'$, $^{13}C\alpha$, and $^{13}C\beta$ shifts (mean ± deviation) are 121.0 ± 6.5, 174.3 ± 1.9, 56.4 ± 4.0, and 46.6 ± 16.2 ppm; for the turn residues, 117.2 ± 8.0, 175.5 ± 2.0, 54.5 ± 5.8, and 39.8 ± 15.3; and for the helical residues, 119.8 ± 2.5, 178.3 ± 1.8, 58.5 ± 4.0, and 32.4 ± 12.4. Clearly the turns were easiest to identify based on the large dispersion of ^{15}N shifts, and the β-strands are similarly well resolved. We did not have any special difficulties assigning the helix of GB1, despite the relatively poor ^{15}N and $^{13}C\beta$ dispersion; we attribute this to the $^{13}C'$ and $^{13}C\alpha$ dispersion in this amphiphatic helix. In general, the assignment of fully helical (membrane) proteins in the solid state will be a special challenge that is likely to require new types of experiments to emphasize inter-residue correlations among side chains, to compensate for the inferior ^{15}N dispersion.

c. Structural Comparisons with Crystallography and Solution NMR. With assignments in hand, we proceeded to analyze the chemical shifts in terms of backbone conformation. Isotropic N, Cα, Cβ, and C′ chemical shifts in proteins are known to depend on secondary structure, both in solution[64] and in the solid state.[11,65] We used TALOS[64] to analyze the ϕ and ψ backbone torsion angles for GB1 in the microcrystalline state (Figure 6). Of the 53 ϕ, ψ pairs (106 total torsion angles) reported by TALOS, 42 ϕ values agreed with the X-ray structure within the TALOS error ($\pm 1\ \sigma$); 4 additional values were within $\pm 2\ \sigma$, and 7 were in poor agreement. Among the ψ values, 42 were with within $\pm 1\ \sigma$, and 6 additional were within $\pm 2\ \sigma$, leaving 5 in poor agreement. The regions of poor agreement (or unreported by TALOS due to lack of convergence) were typically Gly residues (G9, G14, G41), residues neighboring Gly residues (N8, K10, D40) and/or residues in turns (D47) between well-defined secondary structure elements. Other than in these regions, the GB1 chemical shifts in the microcrystalline state predict a backbone structure that agrees remarkably well with the crystal structure. In the regions where TALOS fails, direct backbone torsion angle determinations[20,66] and chemical shift anisotropy (CSA) measurements[21] will be beneficial for structure determination and refinement. We have recently performed such a study of CSA measurements in GB1.[67]

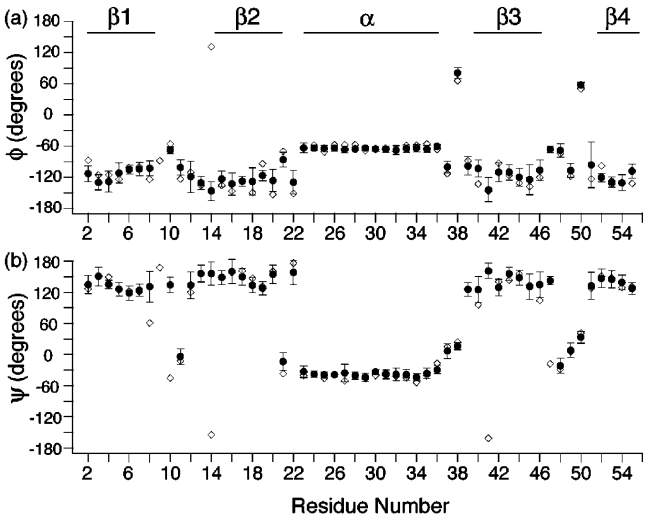

Figure 6. TALOS-based analysis of backbone torsion angles in microcrystalline GB1.[64] The open diamonds illustrate the crystal structure backbone torsion angle values. The solid circles are shown in the 106 cases where TALOS converged, with the error bars as reported by TALOS.

To examine the conformation of the side chains, we proceeded to analyze the variation between solid-state and solution chemical shifts. The solid-state chemical shifts were determined in most cases to ±0.1 ppm or better certainty, based upon the statistical variation in several data sets. The solution shifts were determined to a digital resolution of better than 0.1 ppm under conditions as close as possible to those of the solid sample (see Experimental Section). The differences in chemical shift by residue number (Figure 7) show that the overall agreement between solution and solid shifts is within this uncertainty. Moreover, the standard deviation in the chemical shift differences is in the case of $^{13}C\alpha$ and $^{13}C'$ signals two times larger than the mean shift difference, and for $^{13}C\beta$ and ^{15}N signals the standard error is substantially larger than the mean shift difference. The $^{13}C\beta$ signals demonstrating the largest differences are Cβ-branched (T17, V39, and T55), aromatic (W43 and Y45), or charged (K13, D36, D40, and K50) residues. Further, several of the discrepancies, both for aromatic and nonaromatic $^{13}C\beta$ signals, are clustered in the region near residues 39 to 45 (e.g., V39, D40, W43, and Y45). Likewise for the ^{15}N signals, although there are several ppm variations with no obvious pattern throughout much of the protein (due presumably to the strong dependence of ^{15}N chemical shifts on electrostatic environment), the region from residues 42 to 48 shows a systematic trend of positive values in Figure 7d, corresponding to an upfield shift in the solid sample relative to solution. This is near a region (residues 39−46) in which the C′ shifts show a downfield ∼1 ppm trend in the solid relative to solution (Figure 7c).

Insight into these effects can be derived from comparisons to the crystallography studies of Gallagher, in which it was noted that the rotameric states of several Lys, Glu/Gln, and Asn residues depended on crystal packing.[32] Therefore changes in

(64) Cornilescu, G.; Delaglio, F.; Bax, A. *J. Biomol. NMR* **1999**, *13*, 289−302.
(65) Luca, S.; Filippov, D. V.; van Boom, J. H.; Oschkinat, H.; de Groot, H. J. M.; Baldus, M. *J. Biomol. NMR* **2001**, *20*, 325−331.
(66) Rienstra, C. M.; Hohwy, M.; Mueller, L. J.; Jaroniec, C. P.; Reif, B.; Griffin, R. G. *J. Am. Chem. Soc.* **2002**, *124*, 11908−11922.
(67) Wylie, B. J.; Franks, W. T.; Graesser, D. T.; Rienstra, C. M. *J. Am. Chem. Soc.*, published online August 4, http://dx.doi.org/10.1021/ja053862e.

Table 1. ^{15}N and ^{13}C Chemical Shifts of Microcrystalline GB1

res	N	C′	Cα	Cβ	Cγ	Cδ	Cϵ	Cζ	Nδ	Nϵ	Nζ
M1	40.0	171.4	54.3	32.5	30.3		15.9				
Q2	125.2	175.1	55.9	30.5	35.3	180.4				113.2	
Y3	123.3	175.0	57.0	43.7	128.5	134.7	118.3	158.3			
						132.0	118.3				
K4	122.7	173.3	54.9	36.3	25.7	29.1	42.4				33.1
L5	127.0	174.8	53.0	42.5	27.4	26.0					
						25.1					
I6	126.3	175.3	60.0	37.9	27.5	12.8					
					17.6						
L7	127.1	175.1	54.7	42.9	27.2	26.9					
						25.1					
N8	125.1	176.4	50.7	38.4	176.6				110.9		
G9	109.6	173.2	44.6								
K10	121.1	179.2	59.3	32.9	25.8	29.2	42.1				33.1
T11	106.4	173.4	61.9	69.5	22.6						
L12	127.8	173.9	54.4	43.1	27.9	26.1					
						23.0					
K13	123.3	175.8	53.3	38.8	26.1	29.8	43.0				31.3
G14	105.6	171.4	44.9								
E15	121.1	174.1	53.9	34.2	35.1	181.9					
T16	115.2	172.0	60.1	70.5	20.1						
T17	116.1	174.3	60.3	72.6	21.8						
T18	116.3	171.3	61.3	70.8	18.9						
E19	125.4	175.9	54.3	30.6	35.8	182.2					
A20	125.9	177.8	50.7	23.7							
V21	116.3	175.1	63.5	32.0	20.2						
					21.2						
D22	115.5	175.1	52.5	42.3	179.9						
A23	122.8	179.7	54.6	18.2							
A24	120.8	181.5	54.5	18.2							
T25	117.4	175.9	67.2	67.8	21.4						
A26	124.0	177.3	55.0	17.6							
E27	116.4	177.8	59.1	29.1	35.5	181.7					
K28	117.4	179.2	60.2	32.8	30.1	26.5	42.3				32.6
V29	119.3	179.0	66.3	32.0	22.2						
F30	118.7	179.1	57.5	37.5	138.4	132.3	130.9				
K31	120.8	179.6	60.1	31.6	27.3	29.3	41.2				32.2
Q32	121.3	177.6	58.9	29.0	34.2	180.0				115.6	
Y33	121.0	178.8	61.6	37.0	129.8	132.5	118.7	159.4			
A34	122.7	179.6	56.1	18.1							
N35	118.2	179.6	57.0	39.3	176.1				113.2		
D36	121.1	176.2	55.9	38.3	177.8						
N37	115.0	174.3	53.5	40.4	176.9				114.6		
G38	108.4	174.0	46.8								
V39	121.8	175.2	61.7	32.0	22.0						
					18.2						
D40	131.1	174.9	52.8	41.7	180.7						
G41	108.1	172.8	45.1								
E42	119.0	177.9	55.1	31.5	35.7	181.8					
W43	125.0	177.4	57.5	33.8	111.8	127.2	138.5	114.7		131.7	
						129.7	119.9	120.6			
T44	109.2	174.0	60.9	73.1	21.1						
Y45	118.6	171.9	57.8	37.6	127.8	132.5	118.8	157.5			
						132.2	116.2				
D46	126.3	176.3	50.9	42.6	180.2						
D47	123.4	177.5	54.6	43.0	179.8						
A48	119.0	179.7	54.0	19.0							
T49	104.2	175.8	60.3	69.9	21.6						
K50	119.7	175.5	55.6	28.0	24.4	28.3	43.3				33.9
T51	112.0	174.4	62.5	71.7	21.3						
F52	130.3	175.8	56.6	43.1	140.0	131.6	130.5				
T53	112.2	172.3	60.4	71.9	21.1						
V54	118.4	172.6	58.5	32.7	21.9						
					19.8						
T55	124.1	174.2	61.3	72.1	21.5						
E56	131.1	180.5	57.6	38.8	183.2						

the chemical shifts of these signals, which are also strongly dependent on local electrostatic environment, are not surprising. Second, branched chain and aromatic amino acids have modest energetic barriers between conformational states; i.e., these may be very small in comparison to the crystal packing forces or even thermal fluctuations, enabling a facile interconversion (as investigated further below). Third, the interaction between β-strands 2 (β2) and 3 (β3) forms a major part of the crystal contact in the orthorhombic crystal form of GB1. Several of the residues that show the largest shifts between solution and

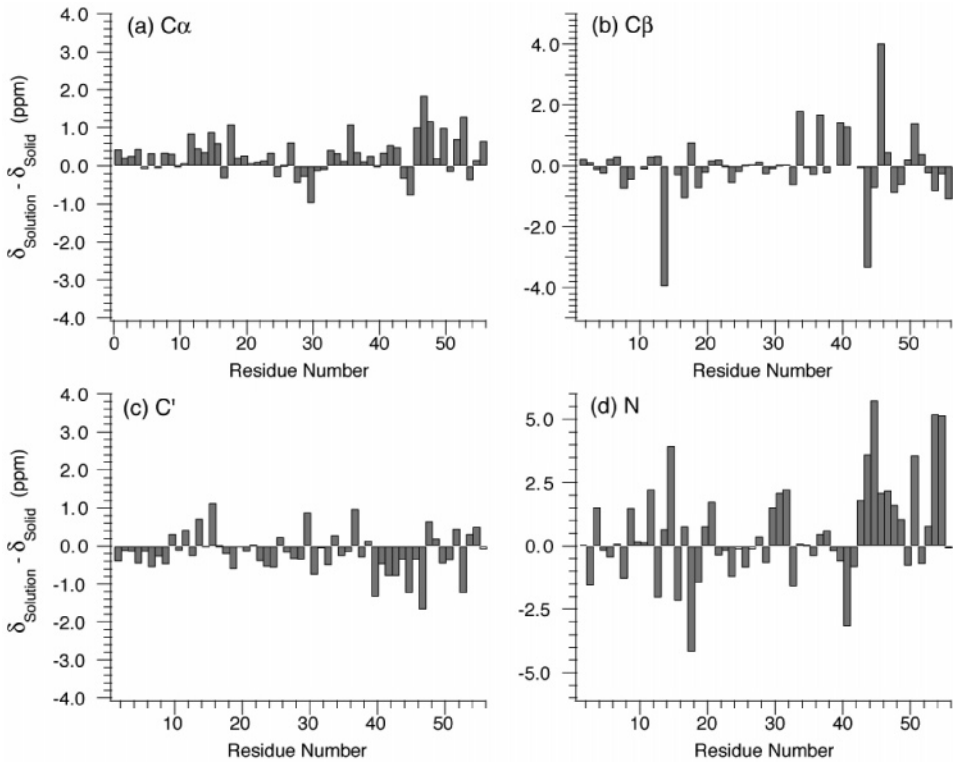

Figure 7. Comparison of isotropic chemical shifts of GB1 in solution and in the microcrystalline solid state. (a) $^{13}C\alpha$. The mean ± standard deviation difference (solution minus solid) was 0.23 ± 0.52 ppm. (b) $^{13}C\beta$: −0.07 ± 1.13 ppm (c) $^{13}C'$: −0.20 ± 0.55 ppm (d) ^{15}N: 0.56 ± 2.00 ppm.

solid are indeed in β2 (K13, T17), in β3 (D40, W43, Y45), or near the end of the helix and/or turn connecting the helix to β3 (D36, V39).

From these chemical shift data comparing solid GB1 to crystal and solution NMR structural parameters, we conclude that the backbone conformations in all three cases are the same within the error of our measurements. Relatively few side-chain chemical shift differences are observed between GB1 in the solid state and in solution, and those variations are strongly correlated to the sites of crystal contacts. Therefore for purposes of further analysis of dynamics in this work, we assume that the overall structure in the microcrystalline state is well described by the crystal structure. This conceptual framework explains several additional observations in the NMR data, as discussed further in the following sections.

d. Effective Backbone $^{1}H-^{15}N$ and $^{1}H-^{13}C\alpha$ Bond Lengths. The variations in integrated intensity among sites in both the $^{13}C-^{13}C$ and $^{15}N-^{13}C$ spectra led us to consider the extent to which backbone and/or side-chain dynamics might affect the rates of polarization transfer in dipolar recoupling experiments. To measure the $^{1}H-^{15}N$ and $^{1}H-^{13}C$ dipolar couplings, dipolar-shift (DIPSHIFT)[68,69] experiments were implemented in a 3D fashion, using ^{15}N and $^{13}C\alpha$ as the two chemical shift dimensions, and a constant time T-MREV period for heteronuclear $^{1}H-X$ recoupling (Figure 8).[70]

Variations in the couplings derived in DIPSHIFT experiments can arise either from changes in bond lengths[71,72] or small amplitude librational dynamics; the latter effect is analogous to order parameters measured in solution NMR. Among the $^{1}H-^{13}C$ sites measured and fit well to the analytical T-MREV model, all but a few were within error of the scaled dipolar coupling expected for a rigid lattice sample (~10.4 kHz; some of the uncertainty is inherent to the scaling factor, which varies due to B_1 inhomogeneity). Significantly below average couplings in the $^{1}H-^{15}N$ spectra were observed at sites D40, G41, W43, and V54. D40 and G41 are in the turn between the helix and β3; W43 (in β3) and V54 (in β4) are in close contact and may exhibit weaker than normal couplings due to H-bond stretching across the β-strand, although this is at the edge of statistical certainty in the current data. Nevertheless, most backbone sites exhibit $^{1}H-^{15}N$ and $^{1}H-^{13}C\alpha$ couplings consistent with a rigid lattice. The mean scaled (±standard deviation) $^{1}H-^{15}N$ coupling is 4784 ± 353 Hz, and the mean scaled $^{1}H-^{13}C\alpha$ coupling is 9804 ± 476 Hz.

Larger variations are observed in the relaxation rates of coherences involving protons, as extracted from the T-MREV spectra. The relaxation rate $\Gamma 2$ (in the formulation of ref 66) reports on the rate of decay of antiphase coherence involving the X (^{13}C or ^{15}N) and ^{1}H spin. In the GB1 data, this value (mean ± standard deviation) is 4.2 ± 3.0 ms^{-1} for $^{1}H-^{13}C$ and 3.0 ± 2.4 ms^{-1} for $^{1}H-^{15}N$. We conclude therefore that the variations in maximum $^{13}C\alpha$ *intensity* from site to site (as discussed in section *b* above) arise primarily from variations in relaxation rates during $^{1}H-^{15}N$ and $^{15}N-^{13}C$ cross polarization. Factors influencing ^{1}H rotating frame relaxation, such as nearby chemical exchange events involving protons, are likely additional contributors to these variations in $^{1}H-^{15}N$ CP efficiency.

(68) Munowitz, M. G.; Griffin, R. G.; Bodenhausen, G.; Huang, T. H. *J. Am. Chem. Soc.* **1981**, *103*, 2529−2533.
(69) Munowitz, M. G.; Griffin, R. G. *J. Chem. Phys.* **1982**, *76*, 2848−2858.
(70) Hohwy, M.; Jaroniec, C. P.; Reif, B.; Rienstra, C. M.; Griffin, R. G. *J. Am. Chem. Soc.* **2000**, *122*, 3218−3219.
(71) Roberts, J. E.; Harbison, G. S.; Munowitz, M. G.; Herzfeld, J.; Griffin, R. G. *J. Am. Chem. Soc.* **1987**, *109*, 4163.
(72) Song, X. J.; Rienstra, C. M.; McDermott, A. E. *Magn. Reson. Chem.* **2001**, *39*, S30−S36.

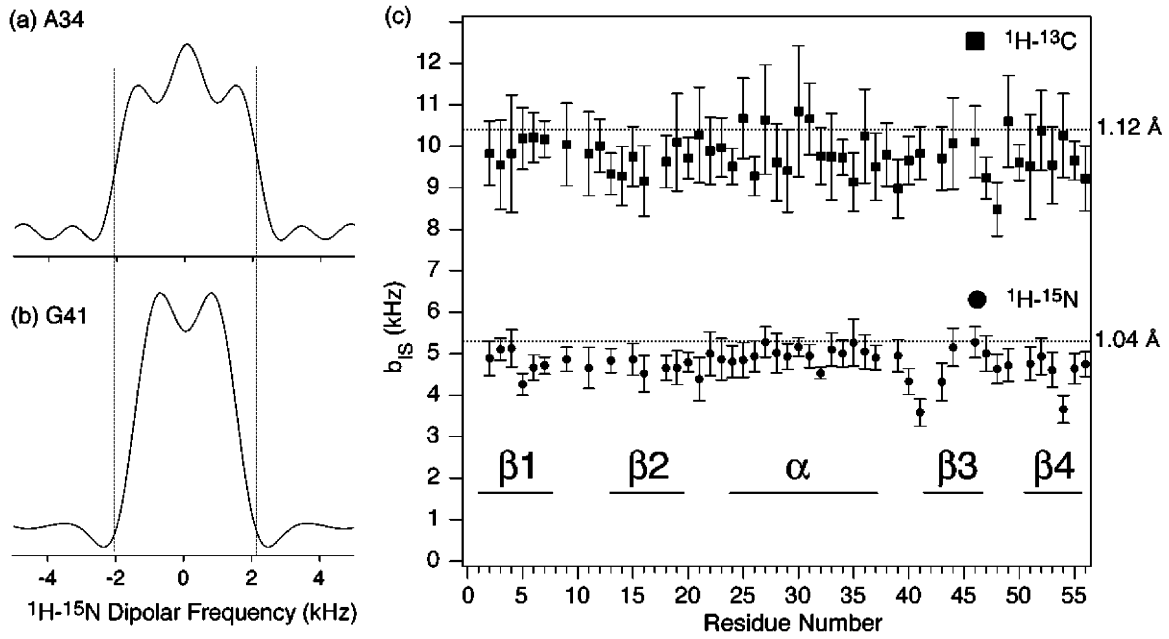

Figure 8. Measurements of GB1 ^{1}H−^{15}N and ^{1}H−^{13}Cα backbone dipolar couplings from 3D DIPSHIFT spectroscopy.[66,68−70] A series of 2D ^{15}N−^{13}Cα spectra (∼45 min each) were acquired as a function of the ^{1}H−^{15}N and ^{1}H−^{13}C T-MREV mixing times (in separate experiments).[66] The resulting site-resolved dephasing trajectories were fit to the analytical model for T-MREV dephasing.[70] (a and b) Examples of ^{1}H-dephased ^{15}N-observe dipolar spectra for (a) A34 and (b) G41; the A34 line shape is consistent with the rigid lattice limit, whereas G41 demonstrates a ∼75% scaling of the dipolar coupling due to small amplitude backbone librations and/or ^{1}H−^{15}N bond stretching (note that this corresponds to an order parameter, S^2, of ∼0.5). The vertical lines are to guide the eye only; dipolar coupling values were extracted from numerical simulations. (c) Summary of fitted ^{1}H−X dipolar couplings; error bars shown are ±2 σ.[66,70] Effective bond lengths of 1.12 Å (^{1}H−^{13}Cα) and 1.04 Å (^{1}H−^{15}N), with a T-MREV scaling factor of 0.48,[66,70] yield couplings of 10.4 and 5.3 kHz, respectively, for ^{1}H−^{13}Cα and ^{1}H−^{15}N, as indicated by the horizontal, dotted line. Variations in the fitted dipolar coupling b_{IS} can arise from changes in this presumed bond length (e.g., stretching due to hydrogen bonding effects) or librational dynamics of larger than average amplitude. Reductions of both the ^{1}H−^{13}C and ^{1}H−^{15}N coupling constants at the same residue are evidence of dynamics. Data points missing from the plot include those signals overlapped in the 2D ^{15}N−^{13}Cα plane and the dephasing trajectories that yielded unsatisfactory fits (>10% RMSD).

e. Side-Chain Conformational Exchange. As mentioned above, the 2D ^{13}C−^{13}C spectra also revealed significant variations in side-chain signal intensities within residue types. We performed more detailed investigations of the Val and Tyr residues in GB1, since these were among the signals that demonstrated the largest variations in intensities and line widths, yet were mostly resolved in the 2D ^{13}C−^{13}C spectra at 500 MHz, enabling quantification of cross-peak intensities. For example, three of the four Val Cα−Cβ correlations (21, 29, and 39) are resolved in the 2D ^{13}C−^{13}C spectra (e.g., Figure 3 and Figure 9a). Among these, V29 has the greatest intensity (normalized to 100%, with a signal-to-noise ratio of ∼45:1) and line widths of 106 Hz (Cα) and 95 Hz (Cβ, in the SPC-5$_3$ spectrum processed with a net 20 Hz Gaussian broadening). In the same spectrum, V39 has 70% of the intensity and line widths of 112 and 113 Hz. V21 has 45% of the normalized intensity and line widths of 116 and 143 Hz. (The same effects are observed to within a 10% error if the Cβ−Cα peaks are considered.)

We next investigated whether side-chain conformational exchange might be responsible for the signal variations, in context of the crystal structure (Figure 9b). V29 is within the very well-ordered amphipathic helix; therefore, it is expected to have the least conformational flexibility among the three residues considered here, which is confirmed by its intensity in the 2D SPC-5$_3$ spectrum (Figure 9a). V39 is in a turn between the helix and the β3-strand, but its side chain is packed into the core of the protein against other hydrophobic side chains; it is therefore an intermediate case, where the signal in the SPC-5$_3$ spectrum is reduced relative to V29. Although the V39 shows very similar Cα−Cβ transfer rates and intensities to V29 (Figure 9b), its Cα−Cγ transfer is significantly attenuated in intensity. V21 is in a turn between β2 and the helix, and its side chain is in a crystal contact, explaining larger broadening observed on the Cβ signal. The V21 Cα−Cβ transfer *rate* is slightly reduced in comparison to V29 and V39, and the decrease in *intensity* is even more prominent; both dipolar transfer rates and intensities are substantially reduced for the Cα−Cγ cross-peaks. Thus the backbone motion is the minor and the side-chain motion is the major contribution to attenuation in signal intensity.

The Val side-chain chemical shifts corroborate these observations, when compared empirically to the stereospecific assignments of the prochiral methyl carbons of Leu and Val residues in malate synthase G (MSG)[73] and a recent solution NMR study of methyl-bearing side chains in GB3.[74] We constructed an empirical database from the chemical shifts of MSG Val residues and found the best agreement (RMSD minimum) between GB1 and MSG chemical shifts identified by residue. The ^{13}C chemical shifts V21 of GB1 were found to be most similar to V275 and V377 of MSG, both of which have undefined χ_1 values. This is consistent with a study of the closely related protein GB3, in which it was established that V21 exhibits rotameric averaging; Kalplus analysis identified asymmetric populations among the three possible conformers (23% $\chi1 = 180°$, 57% $\chi1 = -60°$, and 20% $\chi1 = +60°$), and residual dipolar data were most consistent with 50% $\chi1 = 180°$, 50% $\chi1 = -60°$. Moreover,

(73) Tugarinov, V.; Kay, L. E. *J. Am. Chem. Soc.* **2004**, *126*, 9827−9836.
(74) Chou, J. J.; Case, D. A.; Bax, A. *J. Am. Chem. Soc.* **2003**, *125*, 8959−8966.

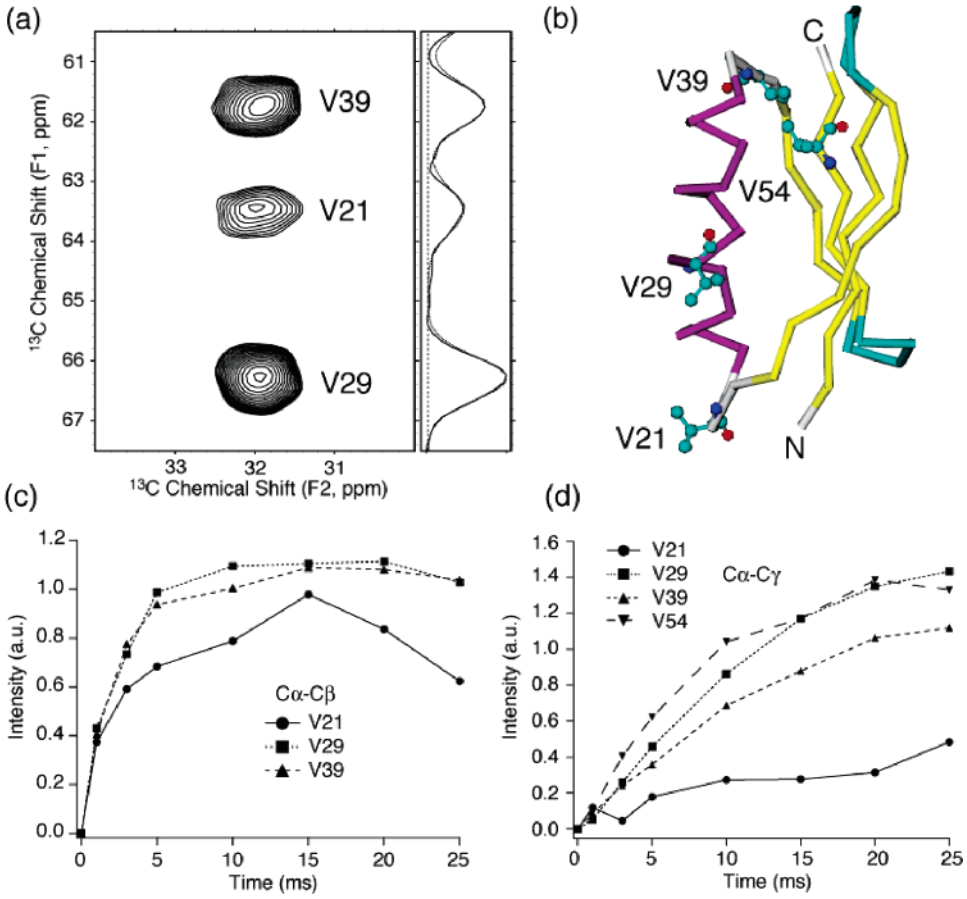

Figure 9. Signal intensity and dipolar transfer rates exhibited by Val residues in GB1. (a) Val Cβ-Cα region of the SPC-5_3 spectrum (expansion of Figure 3a) and slice through the F1 dimension at F2 = 32.0 ppm, illustrating the variations in signal intensity. (b) Cartoon of the GB1 structure illustrating the location of the Val residues. (c) Buildup of Cβ polarization originating from the Cα, as a function of DARR mixing time. The spectra were acquired by varying the DARR mixing time, with other parameters described in the caption to Figure 2. (The V54 Cα-Cβ peak was not sufficiently well resolved to quantify its intensity in these spectra.) (d) Buildup of Cγ polarization originating from Cα, as a function of DARR mixing time (from the same spectra as part c). In cases where both Cγ signals were resolved (V21, V29, and V54), the average intensity is reported; for V39, the intensity of the single resolved C$\alpha-$Cγ peak at 61.7, 18.2 ppm is reported.

the side-chain crystal structures for GB1 have different χ_1 angles for this residue (in the wild type 1pga structure, $\chi 1 = -60°$, and in the T2Q mutant, $\chi 1 = +60°$). Our data are consistent with fast-limit $\chi 1$ conformation exchange of the V21, but the distinct Cγ peaks require unequal populations of the three conformers. The other Val residues do not show such dynamic properties and have chemical shifts that can be interpreted in terms of side-chain conformation unambiguously. The V29 and V39 chemical shifts are consistent with trans conformations ($\chi_1 = \sim 180°$), as in the crystal structures. Both the upfield-shifted Cα (58.5 ppm) and side-chain shifts of V54 are consistent with a g+ conformation ($\chi_1 = 60°$), as in residues V446 and V608 of MSG. We have in another study investigated the effects of this conformation upon chemical shift tensor magnitude; the span of the Cα CSA tensor for this residue is ~6 ppm greater than V39, in agreement with this g+ conformation.[67]

A second example of side-chain conformational dynamics arises from examination of Tyr ring cross-peak intensities as a function of ^{13}C$-^{13}$C mixing time (Figure 10). For Y3 and Y45, the C$\zeta-$Cϵ cross-peaks arise quickly (at 5 ms mixing), and at the longer mixing time (50 ms) two sets of Cϵ and Cδ peaks are observed for Y45. The dipolar transfer from the Cζ to Cϵ of Y33 is slower, with a large fraction of the polarization remaining on the Y33 Cζ at 5 ms. At the longer mixing time, transfer occurs to the Cϵ and Cδ signals (the Cϵ1 and Cϵ2 occur at a common chemical shift, as do the Cδ1 and Cδ2). These observations again are consistent with, and elaborate upon, the GB1 crystal structure, in which Y45 and Y3 are tightly packed in the hydrophobic core (along with F30, F52, and W43), and the hydroxyl proton of Y45 participates in a hydrogen bond with D47, further constraining its ring conformation. In contrast, the ring of Y33 is closer to the protein surface; the SSNMR data illustrate that this aromatic ring is undergoing two-site exchange on a time scale of $>10^6$ s^{-1} (χ^2 $\pm 180°$).[75,76]

These observations near room temperature directly confirm the presence of conformational exchange in GB1, an effect that changes signal intensities and line widths, but does not depress the signals below the limit of detection.

f. Temperature-Dependent Chemical Shift Spectra. Having identified sites of conformational exchange near room temperature, we proceeded to acquire spectra at lower temperatures. The overall trends in signal intensities and line widths can be appreciated most readily from the 1D experiments over a

(75) Rice, D. M.; Meinwald, Y. C.; Scheraga, H. A.; Griffin, R. G. *J. Am. Chem. Soc.* **1987**, *109*, 1636−1640.
(76) Rice, D. M.; Wittebort, R. J.; Griffin, R. G.; Meirovitch, E.; Stimson, E. R.; Meinwald, Y. C.; Freed, J. H.; Scheraga, H. A. *J. Am. Chem. Soc.* **1981**, *103*, 7707−7710.

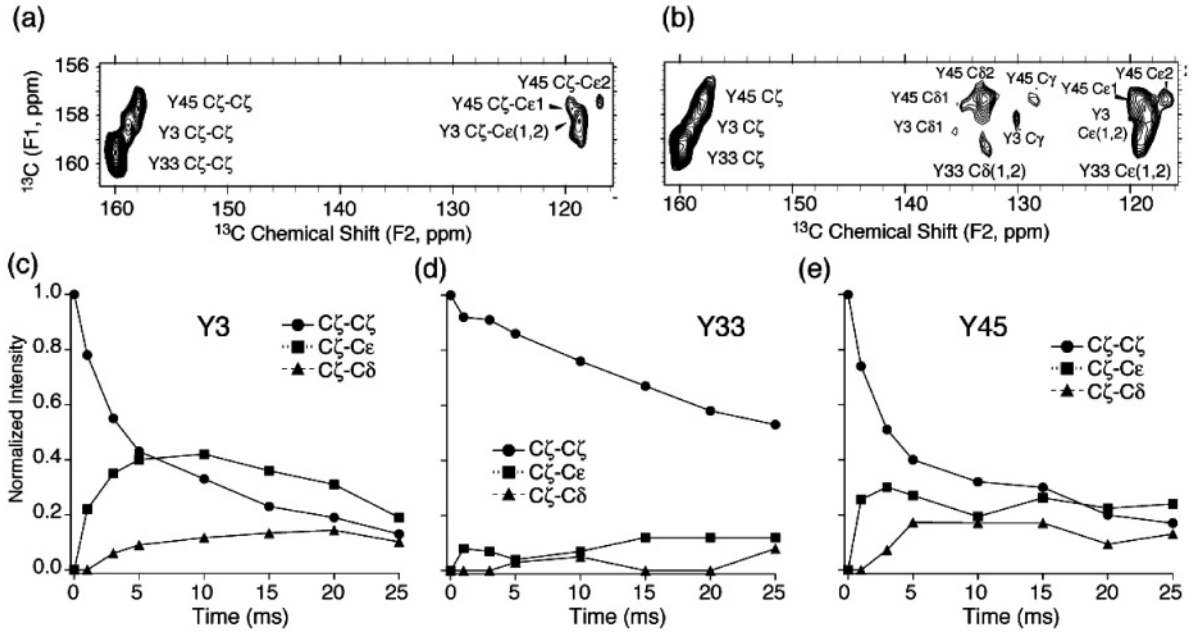

Figure 10. Chemical shift and dipolar trajectories for Tyr residues in GB1. (a and b) Aromatic regions of 2D $^{13}C-^{13}C$ with (a) 5 ms and (b) 50 ms DARR mixing. (c−e) Polarization transfer trajectories as labeled on the figure for (c) Y3, (d) Y33, and (e) Y45. The intensities were normalized to the intensity of the Cζ−Cζ autocorrelation peak.

temperature range from ∼275 to 175 K (Figure 11). As the temperature is lowered from 275 to 204 K, there is a continual degradation in spectral quality that is most evident among terminal, loop, and side-chain resonances. For example, the first signal to fall below our detection sensitivity is the M1 $^{15}NH_3$ (at 240 K); the $^{13}C\epsilon$ signal (15.8 ppm) of M1 likewise is depressed and broadened, although it is not completely lost. Similarly, the Y33 $^{13}C\zeta$ (furthest downfield signal among aromatics) is especially sharp at the highest temperature, showing resolved multiplet structure, but is depressed several fold in intensity at 222 K. The Thr Cβ region retains most of its signal intensity but broadens in a manner similar to that of the Tyr Cζ. The backbone ^{15}N signals overall decrease in intensity by factors of 3 to 5. Even those ^{15}N signals in the hydrophobic core show the same effect, as does the I6 Cδ1, which is packed within the hydrophobic core; however, the magnitude of the broadening and signal attenuation is not as substantial in those cases (a 2- to 3-fold reduction in intensity and increase in line width).

Our observation of deteriorations in spectral quality in the range from 275 to 225 K are qualitatively similar to the observations of Zilm and co-workers in ubiquitin.[52] However, in their studies, broadening continued as the temperature was lowered below 200 K. In GB1, the effect appears to be reversed in this temperature range. We attribute this to the relatively high concentration of MPD in our preparation, which has been shown to provide sufficient cryoprotection to favor a glass transition rather than the freezing of solvent.[77] The temperature range over which this transition occurs is consistent with the characteristic value at which temperature-dependent Debye−Waller factors exhibit a change in slope.[78] The exact temperature at which the SSNMR line width is maximized is expected when solvent translational diffusion interferes with magic-angle spinning and ^1H decoupling, i.e., ∼10−100 kHz.[79] Computed translational diffusion constants for water in myoglobin crystals are ∼25 000 Å^2/s at 220 K.[80] Using an empirical definition that a solvent molecule is in contact with a ^{13}C or ^{15}N site if within 5 Å, the rate of solvent passage through this window would be ∼1000/s, which agrees satisfactorily with the Rothwell−Waugh condition of maximal homogeneous broadening.[79]

2D $^{13}C-^{13}C$ and 3D $^{15}N-^{13}C\alpha-^{13}CX$ spectra as a function of temperature (not shown) were analyzed and summarized by amino acid (Figure 12). At 250 K, K4, T11, K13, E19, V21, K28, and D40 show substantially depressed intensities (signals less than half their values at room temperature). These signals are predominantly in turns. At 240 K, additional resonances in β2 (E15, T16, T17, T18) and β3 (E42, W43, T44) show depressed intensities. These strands form the intermolecular contact in the orthorhomobic crystal form of GB1 and are exposed to solvent.[32] The signals from the helix that are most depressed are K28 and Y33, both of which are on the polar, solvent-exposed side of the amphipathic helix. We have attempted to acquire a variety of $^1H-^{15}N$ correlation spectra to probe protein−solvent interactions directly,[23,42,81] but our efforts so far have not yielded resolved spectra. It is not yet clear whether this is due to an instrumental or fundamental issue.

Another contribution to the observed broadening at ∼200−220 K is side-chain motion on the intermediate time scale. This does not appear to be a major contribution, since, at 175 K, the methyl and aromatic regions of the ^{13}C spectra are identical with the 275 K spectra. If the motional processes discussed above (Y33 ring flipping, V21 side-chain rotameric averaging) were deactivated at the lower temperature, one would expect to see broadening in the intermediate regime and then new chemical shift values in the slow limit. We do not observe

(77) Petsko, G. A. *J. Mol. Biol.* **1975**, *96*, 381−392.
(78) Tilton, R. F.; Dewan, J. C.; Petsko, G. A. *Biochemistry* **1992**, *31*, 2469−2481.
(79) Rothwell, W. P.; Waugh, J. S. *J. Chem. Phys.* **1981**, *74*, 2721−2732.
(80) Tournier, A. L.; Xu, J. C.; Smith, J. C. *Biophys. J.* **2003**, *85*, 1871−1875.
(81) Chevelkov, V.; van Rossum, B. J.; Castellani, F.; Rehbein, K.; Diehl, A.; Hohwy, M.; Steuernagel, S.; Engelke, F.; Oschkinat, H.; Reif, B. *J. Am. Chem. Soc.* **2003**, *125*, 7788−7789.

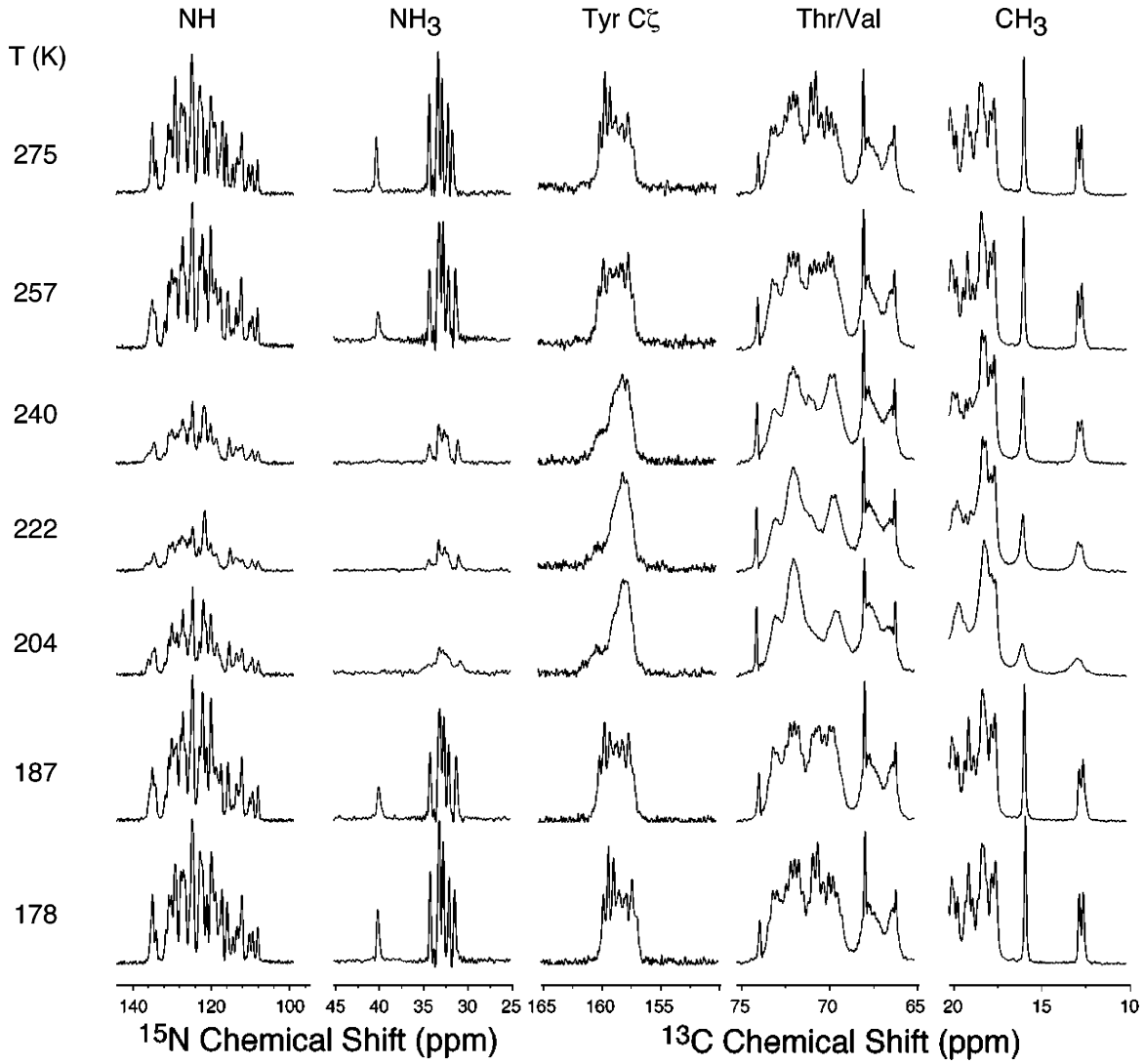

Figure 11. 1D ^{13}C and ^{15}N CP-MAS spectra of GB1 over a range of temperatures as indicated on the figure. Spectra were acquired at 600 MHz ^{1}H frequency, 13.333 kHz MAS rate over a several hour period (~15 min per spectrum). At each temperature, the sample was equilibrated for ~10 min, the probe tuning adjusted, and cross polarization and decoupling conditions were optimized within the same local region of the parameter space, according to the ~5−10% changes in pulse widths over the temperature range. Each vertical series is normalized to the same absolute intensity. The temperature calibration has an uncertainty in absolute temperature of ±5 K due to frictional and rf heating effects, although the relative temperatures are precise to within ±2 K.

Figure 12. Schematic of GB1 amino acid sequence, indicating sites where ^{15}N, $^{13}C\alpha$, $^{13}C\beta$, and $^{13}C'$ signals are substantially depressed in intensity relative to 280 K spectra (underlined and highlighted) or missing entirely (italics) at the sensitivity limit of our 3D $^{15}N-^{13}C\alpha-^{13}CX$ spectra at the indicated temperature. The blue letters correspond to β-strand residues, black to turns or loops and red to the helix.

significant changes in the chemical shifts of Y33 and V21 at 175 K; furthermore, the patterns of cross-peak intensities (in comparison to the other Tyr and Val residues) agree well with those observed at the higher temperature. Indeed, in a 2D $^{13}C-^{13}C$ spectrum (50 ms DARR mixing time) at 175 K, 850 signals were identified and showed an overall -0.02 ± 0.20 ppm agreement with the ~275 K data sets. The only >0.3 ppm deviations were observed at K4, L5, L7, G9, K13, and D22. Therefore it is possible in these residues that side-chain motional modes are deactivated, but this does not satisfactorily explain the overall pattern of signal intensities observed throughout the protein. Site-resolved relaxation measurements[82] and $^{1}H-^{15}N$ (and/or $^{1}H-^{13}C$) correlation experiments[23,42,81] are likely to yield further insight into this phenomenon.

(82) Palmer, A. G. *Chem. Rev.* **2004**, *104*, 3623−3640.

Conclusions

We have presented the ^{15}N and ^{13}C chemical shift assignments for microcrystalline GB1 in the solid state and analyzed chemical shift and dipolar spectra in terms of conformation and dynamics. This study presents a technical benchmark, in that the data utilized for the assignments came exclusively from a suite of 500 MHz experiments performed in approximately 3 h for each 2D experiment and 12−24 h for each 3D experiment. Previous de novo SSNMR chemical shift assignment efforts required much higher field (750 to 800 MHz) 2D spectra and/or acquisitions times of tens of hours (for the 2D spectra)[11] to several days (for the 3D spectra).[83] We attribute the spectral resolution and sensitivity in our study principally to the favorable physical properties of GB1 (high packing density, thermostability, favorable relaxation properties, and microscopic homogeneity). In addition, two instrumental issues that currently compromise SSNMR studies of microcrystalline proteins in general are thermal damage resulting from high-power ^{1}H decoupling and relatively poor detection sensitivity, in comparison to solution NMR. The thermostability and crystal packing density of GB1 mitigated these concerns in the present study. Instrumental developments may enable similar quality spectra to be acquired in a wider range of protein samples; for example, new scroll-resonator probe designs reduce thermal damage from high power proton decoupling.[84]

Our study also has provided new insight into a common problem observed in SSNMR studies; namely, some protein signals may be severely depressed in intensity or missing entirely in some temperature regimes. This phenomenon of missing signals has been observed in BPTI, SH3, Crh, and ubiquitin.[8−11] Zech and McDermott have recently observed some of the missing signals in ubiquitin at 233 and 245 K,[27] but to our knowledge, several of the residues are still missing. GB1 has a well-ordered backbone, short loops connecting secondary structure elements, and terminal residues within the core of the protein (participating in β-strand interactions); site-specific chemical exchange events, including side-chain modes as well as solvent translation, appear to be present only in the fast limit near room temperature. We believe this explains why all of the ^{13}C and ^{15}N signals are visible in our spectra, whereas in previous examples signals in the loops and/or termini were not observed. This novel characteristic of GB1 makes it ideal as a microcrystalline model protein, since near room-temperature conditions can be utilized. The unique properties of GB1 will also enable complete site-specific analysis in experiments for which information throughout the entire protein sequence is desired and fundamental studies of structural phase transitions and dynamics at low temperature. Although we anticipate that suitable formulations of cryoprotectants will be developed for other micro/nanocrystalline proteins, to our knowledge GB1 is the first example in which such high-resolution SSNMR spectra are observed below the glass transition.

Therefore we expect that the chemical shift assignments of GB1 presented here, in combination with its favorable physical and chemical properties, will encourage its use as a model system for further development of SSNMR protein structure determination methodology and fundamental studies of protein thermodynamics in the solid state.

Acknowledgment. This research was supported by the University of Illinois (startup funds to C.M.R.), the American Chemical Society (Petroleum Research Fund), and the National Science Foundation (CAREER Award, MCB 0347824). The authors thank Prof. Eric Oldfield (University of Illinois) for discussions regarding protein chemical shifts, Dr. Angela Gronenborn (National Institutes of Health) for the gift of the plasmid encoding GB1, Dr. Paul Molitor (VOICE NMR Facility, School of Chemical Sciences, University of Illinois) for technical assistance, Prof. Kevin Gardner (University of Texas, Southwestern Medical Center) for discussions regarding GB1 solution chemical shifts, Drs. John Stringer and Chuck Bronnimann (Varian, Inc.) for advice regarding stable probe and spectrometer performance, Sara A. Stellfox for assistance with the low temperature GB1 experiments, and Ying Li for preparing ubiquitin samples.

Supporting Information Available: Supplemental figures and Discussion. This material is available free of charge via the Internet at http://pubs.acs.org.

JA044497E

(83) Igumenova, T. I.; McDermott, A. E. *J. Magn. Reson.* **2003**, *164*, 270−285.
(84) Stringer, J. A.; Bronnimann, C. E.; Mullen, C. G.; Zhou, D. H.; Stellfox, S. A.; Li, Y.; Williams, E. H.; Rienstra, C. M. *J. Magn. Reson.* **2005**, *173*, 40−48.